Transition from the paramagnetic to the antiferromagnetic state actualized in $FeBr_2$

2004 J. Phys.: Condens. Matter 16 3725

(http://iopscience.iop.org/0953-8984/16/21/021)

INSTITUTE OF PHYSICS PUBLISHING JOURNAL OF PHYSICS: CONDENSED MATTER

J. Phys.: Condens. Matter **16** (2004) 3725–3736 PII: S0953-8984(04)73954-5

Transition from the paramagnetic to the antiferromagnetic state actualized in $FeBr_2$

Nai-Li Di[1,2,5], **Setsu Morimoto**[3] **and Atsuko Ito**[1,4]

[1] Graduate School of Humanities and Sciences, Ochanomizu University, Bunkyo-ku, Tokyo 112-8610, Japan
[2] State Key Laboratory for Magnetism, Institute of Physics and Center of Condensed Matter Physics, Chinese Academy of Sciences, Beijing 100080, People's Republic of China
[3] Faculty of Science, Ochanomizu University, Bunkyo-ku, Tokyo 112-8610, Japan
[4] International Institute for Advanced Studies, Kizugawadai 9-3, Kizu-cho, Soraku-gun, Kyoto-fu 619-0225, Japan

E-mail: dinaili@aphy.iphy.ac.cn

Received 26 December 2003
Published 14 May 2004
Online at stacks.iop.org/JPhysCM/16/3725
DOI: 10.1088/0953-8984/16/21/021

Abstract

The magnetic ordering process of the antiferromagnet $FeBr_2$ has been studied by measuring low-field dc-magnetization, ac-susceptibility and the Mössbauer spectrum. All quantities measured show anomalous behaviour around the Néel temperature $T_N = 14.2$ K. We propose defining T_p ($>T_N$) by the temperature where the magnetization is maximum. Because it is T_p, not T_N, that signifies the onset of magnetic ordering. We indicate that $FeBr_2$ transforms from the paramagnetic to antiferromagnetic (AF) state through an intermediate AF domain state which exists in a certain narrow temperature region ΔT just below T_p. From the fact that ΔT is sample-dependent, we have inferred that the stacking fault of the hexagonal c-layers plays an important role in the formation of the intermediate AF domain state.

1. Introduction

The antiferromagnet $FeBr_2$ has been widely studied, and it was believed that the transition from the paramagnetic to antiferromagnetic state in low magnetic fields is a normal one similar to conventional antiferromagnets [1–3]. In this situation, little attention was paid to the behaviour of $FeBr_2$ in zero and low magnetic fields up to recently. We can only find two brief reports about the behaviour of $FeBr_2$ near the Néel temperature T_N in zero field as results

[5] Address for correspondence: State Key Laboratory for Magnetism, Institute of Physics, Chinese Academy of Sciences, Beijing 100080, PO Box 603, People's Republic of China.

of studies performed from a broad viewpoint: (1) Pouget reported that critical fluctuations were observed in the neutron scattering measurements over a wider temperature region extending to temperatures a little above T_N as compared with conventional antiferromagnets [4], and (2) Pelloth *et al* measured the temperature variation of the Mössbauer spectrum and found that the paramagnetic and magnetically split spectrum coexist in a narrow region just below T_N [5]. Several years ago, we also measured the Mössbauer spectra of $FeBr_2$ and observed a coexistence similar to that reported by Pelloth *et al* near below T_N. At that time, however, we did not perform experiments with other methods to clarify the reason for the coexistence. When we reviewed past publications, we found the pioneering Mössbauer study of $FeBr_2$ made by Fujita *et al* [6]. However, the detailed temperature variation of the Mössbauer spectra around T_N has not been reported. Recently, we studied $FeBr_2$ by performing detailed measurements of low-field dc-magnetization and ac-susceptibility, and found anomalous behaviour at temperatures around and just below T_N. We also re-examined the temperature variations of the Mössbauer spectrum in detail. In a previous paper, we have reported some of our results briefly [7]. We have interpreted the results as that the paramagnetic (para) to antiferromagnetic (AF) transition occurs through an intermediate AF domain state which actualized its existence in $FeBr_2$. In this paper, we report the details of our experimental results by putting emphasis on the behaviour of the Mössbauer spectrum.

2. Preliminary details

2.1. $FeBr_2$

The compound $FeBr_2$ has the CdI_2-type hexagonal structure, and it has been known to establish the antiferromagnetic long range order (LRO) below the transition temperature $T_N = 14.2$ K [1]. In the ordered state, Fe^{2+} spins in the hexagonal c-layer are coupled ferromagnetically. The adjacent ferromagnetic layers are separated by two layers of Br^- ions and are coupled antiferromagnetically. Accordingly, the overall magnetic structure is antiferromagnetic. The spin easy axis is parallel to the hexagonal c-axis. This situation is quite similar to that in the case of $FeCl_2$ if one replaces Br^- by Cl^- except for the anion stacking which is ABAB... for $FeBr_2$ and ABCABC... for $FeCl_2$. It is well known that stacking faults occur easily in $FeBr_2$.

2.2. Samples

As we show below, the behaviour of $FeBr_2$ near T_N is sample-dependent, by which we have been motivated to study it in detail. We prepared powder and single crystal samples as below:

(a) *B-P: fine powder.*
The commercial fine powders of $FeBr_2$ of regent grade as prepared were used.

(b) *B-P(a300): fine powder.*
B-P was annealed at 300 °C for 10 days in an evacuated glass ampule.

(c) *C-S: single crystal.*
The single crystal sample was given to us by Aruga Katori and Katsumata. They grew it by the standard Bridgeman method using powder of $FeBr_2$ prepared by direct reaction of 99.99% Fe metal with HBr gas [8].

(d) *C-P: powder (aggregation of small flakes).*
The powder sample was prepared by grinding a part of the C-S.

All the samples were confirmed as containing no other substance than $FeBr_2$ by x-ray diffraction and/or Mössbauer measurements.

2.3. Experimental methods

We performed magnetization and ac-susceptibility measurements using a Quantum Design SQUID magnetometer. The samples were carefully set in a sample holder so as to be stress-free during thermal cycles. We measured the temperature variations of magnetization for various values of dc-field under zero-field-cooled (ZFC) and field-cooled (FC) conditions. We measured the ZFC-magnetization, M_{ZFC}, on heating the sample to 40 K after cooling it from 40 to 4.5 K in zero field (<5 mOe) and then applying the measuring magnetic field. After completing the measurement of M_{ZFC} at 40 K, we turned to decreasing the temperature and measured the FC-magnetization (M_{FCC}) on cooling in the same field down to 4.5 K. The temperature variation of ac-susceptibilities were measured with an ac-field $H_{ac} = 3$ Oe of frequency 20 Hz in $H_{dc} \sim 0$ Oe (<0.3 Oe) between 4.5 and 40 K during the heating and cooling processes. For single crystal sample C-S, H_{dc} or H_{ac} was applied parallel to the *c*-axis. The temperature of the sample was maintained stable to within ± 0.02 K during each of the measurements.

For the Mössbauer measurements, we prepared powder and single crystal absorbers, the thickness of each being about 10 mg natural iron per 1 cm^2. The single crystal absorber was a platelet with the *c*-plane. Each absorber was carefully mounted in a sample holder so as to be stress-free against thermal cycles. We took the Mössbauer spectra at temperatures between 4.5 and 16 K using a conventional constant-acceleration spectrometer in a transmission arrangement. We calibrated the velocity with a natural Fe-metal absorber (8 mg cm^{-2}) at room temperature: we refer the centre shift to that of Fe-metal, and set the total splitting 10.62 mm s^{-1} of the hyperfine spectrum to correspond to 330 kOe. The line width of the inner two absorption lines is 0.23 mm s^{-1}, which is the resolution limit of our present installations. For the single crystal absorber, we detected the transmitted γ-rays in the direction perpendicular to the platelet, that is, parallel to the *c*-axis. In this geometrical arrangement, the absorption lines corresponding to $\Delta m = 0$ transitions between the sublevels of the 14.4 keV excited state and those of the ground state of the ^{57}Fe nucleus are forbidden to appear, and accordingly those lines do not appear in the spectrum for the single crystal absorber. Thus, the shape of the Mössbauer spectrum for the single crystal absorber is different from that for the powder one. We measured temperatures of the samples with a carbon glass thermometer attached to the sample holder whose temperature was controlled by the electronic controller and was kept stable to less than 0.02 K throughout the measurement. The temperature gradient across the absorber was estimated to be negligibly small.

3. Results

3.1. dc-magnetization

The temperature variations of magnetization of the samples measured with $H_{dc} \geqslant 100$ Oe are intrinsically similar to that of the single crystal sample measured with $H_{dc} \sim 100$ Oe by Bertrand *et al* [3], except for the differences due to the sample forms of fine powder, aggregation of small flakes and single crystal. The M–T curves exhibit an anomaly at 14.3 K corresponding to T_N, where T_N is defined by the temperature at which dM_{ZFC}/dT is maximum according to the usual definition. In this paper, we define T_p by the temperature at which M_{ZFC} is maximum. T_p is 14.6 K for all of the samples. A remarkable difference is not recognized to exist between

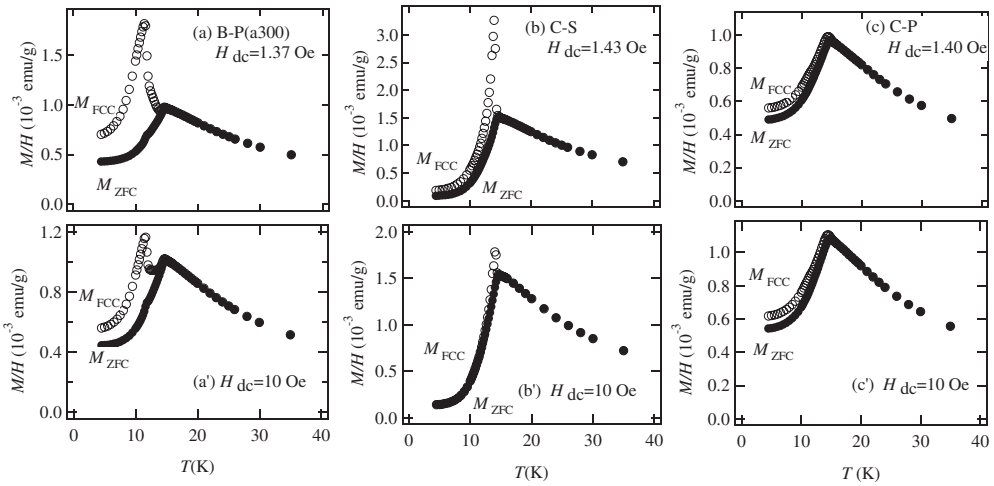

Figure 1. Temperature variations of M_{ZFC}, M_{FCC} for (a) the B-P(a300) sample, (b) the C-S sample, and (c) the C-P sample with ∼1.4 and 10 Oe.

M_{ZFC}–T and M_{FCC}–T curves as $H_{dc} \geqslant 100$ Oe. But, when the applied fields were less than 30 Oe, we found that the behaviour of M_{FCC} below T_N was conspicuously anomalous with decreasing measuring field. Typical examples of the M_{ZFC}–T and the M_{FCC}–T curves for the B-P(a300), C-S and C-P samples at low field $H_{dc} \sim 1.4$ Oe and 10 Oe are illustrated in figures 1(a)–(c) and (a′)–(c′), respectively. One can see how M_{FCC} behaves differently from M_{ZFC}. In addition, it is remarkable that the M_{FCC}–T curve depends largely on the sample.

First, we focus our attention on the behaviour of the sample B-P(a300) shown in figure 1(a). When the temperature is lowered from T_N, M_{FCC} starts to deviate upward from M_{ZFC}, that is $M_{FCC}(T)$ takes larger values than those of $M_{ZFC}(T)$ below T_N. This fact indicates that an excess magnetization, $M_{EX} = M_{FCC} - M_{ZFC}$, appears below T_N when the sample is cooled in magnetic fields. M_{EX} exhibits a maximum at 11.49 K. Henceforth, we refer to the sharp peak of M_{EX} appearing below T_N as the excess peak (EP), and the EP temperature as T_{EP}. We want to remark here that a small hump is seen also in the M_{ZFC}–T curve figure 1(a) at a temperature corresponding to T_{EP}. The sample B-P shows qualitatively similar behaviour (not shown) to that of the B-P(a300). The relative intensity of M_{EX} to M_{ZFC} at T_{EP} for the B-P is larger than that for the B-P(a300) by about 25% when $H_{dc} = 10$ Oe. This fact indicates that the annealing at 300 °C reduces the excess magnetization. From this we infer that some kind of defect, most likely stacking faults in the present case, exist in the sample and play an important role in causing the excess magnetization, and we suppose that these defects are partly removed by the annealing.

The similar measurements for the single crystal sample C-S were also performed. If the sample exist configuration of the stacking faults and/or defects, they would be less from that of the powder sample, because this sample was carefully prepared by slow cooling from molten state. The result is shown in figure 1(b). Similarly to the case of the powder sample B-P(a300), the M_{FCC}–T curve of the C-S sample shows the existence of the excess magnetization. It is clearly seen that a remarkable difference exists between the M_{EX}–T curve for the B-P(a300) and that for the C-S sample. The peak temperature of M_{EX} of the C-S sample is located at T_{EX}(C–P) = 14.03 K, which is considerably higher than T_{EP}(B–P(a300)) = 11.49 K. Moreover, the width of the excess peak of the C-S sample is much narrower than that of the B-P(a300). In other words, M_{EX} of the B-P(a300) has large values distributed over a wider

temperature region. The anomalous values of M_{FCC} at T_{EP} became visibly smaller for both B-P(a300) and the C-S samples as the fields is increased (figures 1(a′) and (b′)). In order to check whether the difference between the M_{FCC}–T curve for the B-P(a300) and C-S samples is due to the material itself or some kind of defect which might be introduced at the time of the sample preparation, we prepared the powder sample C-P by grinding part of the C-S sample. The M_{ZFC}–T and M_{FCC}–T curves of the C-P are shown in figure 1(c). As seen in the figure, for this sample, the M_{FCC}–T curve deviated upward from M_{ZFC} and no evident peak was exhibited. Through the M_{EX}–T curve we found that the maximum value of the excess-peak is around 11.0 K. For the C-P sample, the M_{FCC}–T curve is almost similar at 1.4 and 10 Oe fields (figures 1(c) and (c′)).

Comparing the results of the C-S and the C-P samples, it is clear that the process of grinding the single crystal sample drastically alters the behaviour of the excess magnetization. It is well known that $FeBr_2$ is easily cleaved along the c-plane. Due to this characteristic, a single crystal is split into small flakes along the c-plane by the grinding process. We are convinced that stacking faults are introduced within the flakes here and there by shear stresses along the c-plane during the grinding process. Thus, the behaviour of M_{FCC} of the sample C-P is largely affected by the stacking faults thus introduced. Putting the results shown above together, we infer that stacking faults are the most probable origin of creating the excess magnetization when $FeBr_2$ samples are cooled in magnetic fields. At the present stage, we have no idea how to explain why M_{EX} appears at different temperatures in the three samples when they are cooled from above.

3.2. ac-susceptibility

In figure 2(a), we show the temperature variations of the ac-susceptibilities of the sample B-P(a300) observed under zero bias dc-field (H_{dc} (bias = 0 Oe)). It is clearly seen that the imaginary part χ'' shows a sharp peak at T_{EP}. The sharp peak of χ'' at T_{EP} decreases as the bias dc-field increases and almost disappears above 1 kOe. Therefore, we are convinced that the origin of the behaviour of χ'' around T_{EP} is different from that of the behaviour of χ'' observed under much stronger magnetic fields [9, 10]. Corresponding to this peak, a small but visible hump is seen in the χ'–T curve. These facts suggest that some kind of cooperative transition occurs around T_{EP} in the spin system. Moreover, surprisingly, another sharp peak of χ'' is observed at little above T_N. This is also anomalous and indicates that the transition from the paramagnetic state to the AF one at T_N or T_p of $FeBr_2$ is different from that in ordinary antiferromagnets, which we touch on briefly in section 4. In the single crystal sample C-S, we also recognize two separate peaks in the χ''–T curve around T_{EP} and T_p although they adjoin to each other (figure 2(b)). Even in the sample C-P, similar two peaks of χ'' are observed, although the peak around 11.5 K is fairly small (figure 2(c)). A discontinuous jump of χ'' seen around 12.5 K in figure 2(b) is sometimes observed. Similar jumps appear in all the samples at several temperatures, in particular, when we measure χ'' under applied bias dc-fields. We infer that this phenomenon is closely related to the cooperative rearrangement of spins. The details of the behaviour of the ac-susceptibility including the jump will be published in a separate paper.

3.3. Mössbauer spectra

The temperature variations of the Mössbauer spectra of the samples B-P(a300), C-S and C-P are shown in figures 3(a)–(c). They are qualitatively similar to one another. A common feature that we want to especially remark on is as follows. When the temperature is lowered,

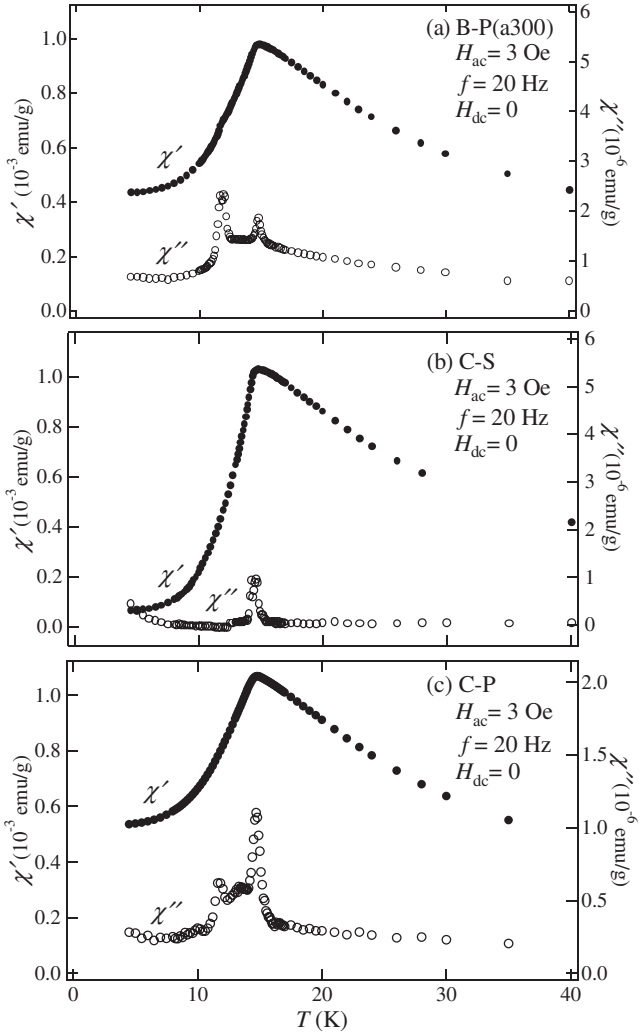

Figure 2. Temperature variations of the ac-susceptibilities (the real part χ' and the imaginary part χ'') for (a) the B-P(a300) sample, (b) the C-S sample and (c) the C-P sample with a frequency of $f = 20$ Hz in a zero bias dc-field.

a magnetically split spectrum (magnetic spectrum) appears around T_p superposed upon a paramagnetic doublet. The intensity of the magnetically split spectrum grows rapidly with decreasing temperature at the expense of the intensity of the paramagnetic doublet. The coexistence of the paramagnetic and magnetic spectra is observed only in a certain narrow temperature region (ΔT) just below T_p. No hysteresis was observed between the spectrum measured on heating and cooling. We performed computer fittings to the observed spectra under the assumption that they consist of two subspectra, a paramagnetic and a magnetic spectrum. The fitting parameters are the hyperfine magnetic field (H_{hf}), the quadrupole splitting ($(1/2)e^2qQ$), the centre shift (δ), and the area ratio of the paramagnetic spectrum to the total absorption (R_{para}). Other Mössbauer parameters θ_H and ϕ_H are the polar and azimuthal angles defining the orientation of H_{hf} relative to the principal axes (x, y, and z) of the electric field

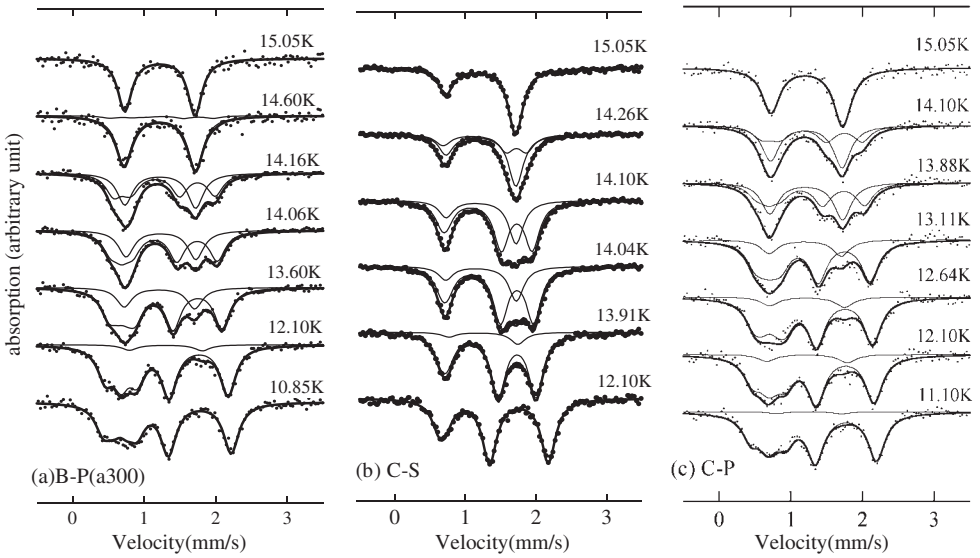

Figure 3. Temperature variations of Mössbauer spectra for (a) the B-P(a300) sample, (b) the C-S sample and (c) the C-P sample. The best fit spectra to the observed ones are shown by solid curves: thin solid curves are the paramagnetic and magnetic sub-spectrum and the thick one is the resultant spectrum.

gradient (EFG) tensors V_{ij} ($V_{ij} = \partial^2 V/\partial^2 T, i, j = x, y, z$), and η ($\eta = (V_{xx} - V_{yy})/V_{zz}$) is the asymmetry parameter of the EFG tensors. In $FeBr_2$, it is known that the z-axis is parallel to the c-axis, the direction of $H_{\rm hf}$ is parallel to the c-axis ($\theta_H = 0$) and η is zero, so that ϕ_H has no meaning [6]. The values of $H_{\rm hf}$, $(1/2)e^2qQ$, δ and $R_{\rm para}$ obtained for the B-P(a300), C-S and C-P samples from the fitting are listed in tables 1–3.

3.3.1. Sample B-P(a300). In figure 3(a), we show the best fit resultant spectrum by the thick solid curve together with the two subspectra of the 0.25 mm s^{-1} line width (thin curves). As seen in the figure, a satisfactory fitting is obtained at each temperature. The temperature variation of $R_{\rm para}$ is shown in figure 4. As the temperature lowers from $T_{\rm p} = 14.6$ K, $R_{\rm para}$ decreases by about 70% within 0.8 K. Then follows a gradual decrease of $R_{\rm para}$ down to zero at around 11 K. That is, the coexistence of the paramagnetic and magnetic spectra is seen over $\Delta T \sim 3.5$ K. In figure 5, the temperature variation of $H_{\rm hf}$ is illustrated. As is seen in the figure; $H_{\rm hf}$ increases with decreasing temperature in a similar manner to that in conventional ferrous magnets. We want to emphasize that no line broadening is observed in the magnetic spectrum over ΔT due to the distribution of $H_{\rm hf}$. In other words, $H_{\rm hf}$ shows no distribution and has a single value at each temperature and it increases as if all spins formed a long-range order (LRO) simultaneously at $T_{\rm p}$, although the paramagnetic doublet changes into the magnetic spectrum below $T_{\rm p}$ successively at the rate shown in figure 4. This fact indicates that, with the temperature decreasing, some paramagnetically fluctuating spins jump to join magnetic order suddenly to show the hyperfine field as same as the magnetic order spins in that temperature. This behaviour gives an important key to understanding what phenomenon happens in the spin system around and just below $T_{\rm p}$. In this paper we do not mention the details of the temperature variation of $(1/2)e^2qQ$ and δ, but we want to point out that $(1/2)e^2qQ$ of the magnetic spectrum is larger than that of the paramagnetic doublet (see table 1) below $T_{\rm p}$, which is consistent with the results reported in [6].

Table 1. The values of $H_{\rm hf}$, $(1/2)e^2qQ$, δ and $R_{\rm para}$ obtained for B-P(a300) from the fitting. Errors are given in parentheses.

T (K)		$H_{\rm hf}$ (kOe)	$(1/2)e^2qQ$ (mm s^{-1})	δ (mm s^{-1})	$R_{\rm para}$
15.05	mag	—	—	—	
	para	0.0[a]	0.95(2)	1.18(3)	1.0[a]
14.60	mag	9.0(5)	0.98(5)	1.01(5)	
	para	0.0[a]	0.97(3)	1.18(3)	0.95(4)
14.38	mag	11.8(3)	0.98(5)	1.03(5)	
	para	0.0[a]	0.97(3)	1.18(3)	0.79(3)
14.26	mag	12.8(3)	0.99(3)	1.02(3)	
	para	0.0[a]	0.97(3)	1.18(3)	0.67(2)
14.16	mag	14.9(3)	1.01(3)	1.01(3)	
	para	0.0[a]	0.96(3)	1.18(3)	0.59(2)
14.06	mag	16.9(3)	1.02(3)	1.01(3)	
	para	0.0[a]	0.96(3)	1.19(3)	0.48(2)
13.60	mag	20.4(3)	1.02(3)	1.01(3)	
	para	0.0[a]	0.95(3)	1.18(3)	0.32(2)
12.60	mag	23.8(3)	1.04(3)	1.00(3)	
	para	0.0[a]	0.98(3)	1.18(3)	0.19(3)
12.10	mag	24.8(3)	1.05(3)	1.01(3)	
	para	0.0[a]	0.99(5)	1.17(5)	0.10(3)
11.40	mag	25.8(3)	1.06(3)	1.01(3)	
	para	0.0[a]	0.99(6)	1.17(6)	0.04(4)
10.85	mag	26.5(3)	1.06(3)	0.99(3)	
	para	—	—	—	0.0[a]
10.39	mag	26.4(3)	1.07(3)	0.99(3)	
	para	—	—	—	0.0[a]
4.50	mag	28.4(3)	1.11(3)	0.99(3)	
	para	—	—	—	0.0[a]

[a] Fixed value.

Table 2. The values of $H_{\rm hf}$, $(1/2)e^2qQ$, δ and $R_{\rm para}$ obtained for the C-S sample from the fitting. Errors are given in parentheses.

T (K)		$H_{\rm hf}$ (kOe)	$(1/2)e^2qQ$ (mm s^{-1})	δ (mm s^{-1})	$R_{\rm para}$
15.05	mag	—	—	—	
	para	0.0[a]	0.96(3)	1.18(3)	1.0[a]
14.26	mag	8.5(5)	1.01(5)	1.17(5)	
	para	0.0[a]	0.96(3)	1.18(3)	0.76(3)
14.10	mag	13.1(3)	1.00(3)	1.17(3)	
	para	0.0[a]	0.96(3)	1.18(3)	0.48(2)
14.04	mag	14.1(3)	0.99(3)	1.18(3)	
	para	0.0[a]	0.97(3)	1.18(3)	0.39(2)
13.91	mag	16.2(3)	1.00(3)	1.18(3)	
	para	0.0[a]	0.95(5)	1.18(5)	0.16(3)
12.10	mag	25.1(3)	1.05(3)	1.18(3)	
	para	—	—	—	0.0[a]

[a] Fixed value.

3.3.2. Sample C-S. The Mössbauer spectra for the C-S sample were also analysed by a similar fitting to the B-P(a300) sample. In figure 3(b), the subspectra line width is 0.24 mm s^{-1}. As is seen in the figure, the fitting curve quite excellently reproduces the measured spectrum at each temperature. This ensures that there is no distribution of $H_{\rm hf}$ over ΔT. In figure 4, it

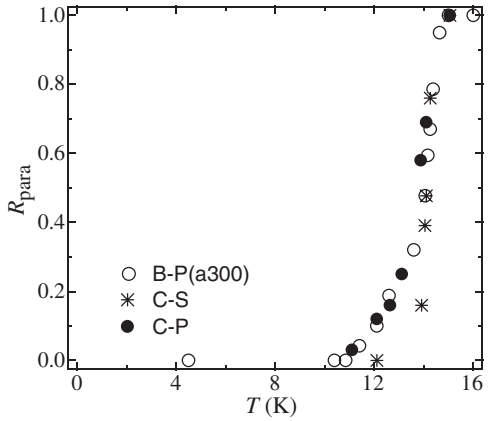

Figure 4. Temperature variation of the area intensity ratio of the paramagnetic doublet to the total absorption area, R_{para}, for the samples of B-P(a300), C-S and C-P.

Table 3. The values of H_{hf}, $(1/2)e^2qQ$, δ and R_{para} obtained for the C-P sample from the fitting. Errors are given in parentheses.

T (K)		H_{hf} (kOe)	$(1/2)e^2qQ$ (mm s^{-1})	δ (mm s^{-1})	R_{para}
15.05	mag	—	—	—	
	para	0.0[a]	0.97(3)	1.15(3)	1.0[a]
14.10	mag	15.6(3)	0.99(3)	0.99(3)	
	para	0.0[a]	0.97(3)	1.15(3)	0.69(2)
13.88	mag	17.7(3)	1.02(3)	0.97(3)	
	para	0.0[a]	0.99(3)	1.14(3)	0.58(2)
13.11	mag	21.6(3)	1.03(3)	0.98(3)	
	para	0.0[a]	0.98(3)	1.13(3)	0.25(2)
12.64	mag	23.5(3)	1.01(3)	0.99(3)	
	para	0.0[a]	1.01(3)	1.16(5)	0.16(3)
12.10	mag	24.3(3)	1.03(3)	0.99(3)	
	para	0.0[a]	1.06(5)	1.15(5)	0.12(3)
11.10	mag	25.5(5)	1.05(5)	0.98(5)	
	para	—	—	—	0.0[a]

[a] Fixed value.

is seen that the region where the paramagnetic and magnetic spectra coexist is fairly narrow for the C-S sample as compared with that for the B-P(a300) sample: ΔT(C-S) $\cong$ 0.8 K (cf ΔT(B-P(a300)) $\cong$ 3.5 K). Interestingly, however, the behaviour of R_{para} at the first 0.8 K downward from T_p is similar for both the samples. This indicates that in the B-P(a300) sample the transient phenomenon extends toward the low temperature side after it proceeds rapidly for the first 0.8 K. The temperature variation of H_{hf} shown in figure 5 is in agreement. This indicates that the temperature variation of H_{hf} is not affected by the difference in the macroscopic behaviour of the magnetization and the ac-susceptibility (see figures 1 and 2).

3.3.3. Sample C-P. The Mössbauer spectra for the C-P sample were also analysed similarly as mention above. In figure 3(c), the subspectra line width is 0.27 mm s^{-1}. Comparing figure 3(c) with (a), one can see that the temperature variation of the spectrum for the C-P sample is quite similar to that for the B-P(a300) sample. The temperature variation of R_{para} for the C-P sample

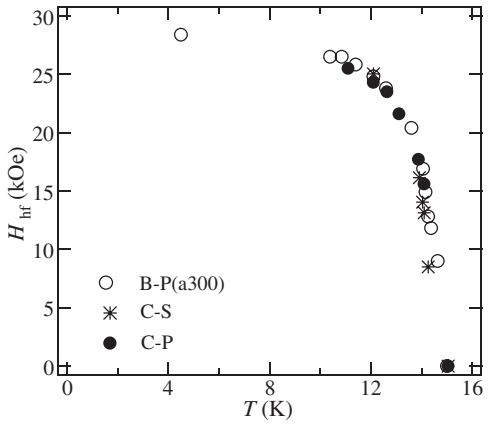

Figure 5. Temperature variation of H_{hf} for the samples of B-P(a300), C-S and C-P.

(figure 4) indicates that a significant difference does not exist. The behaviours of R_{para} for both powder samples are qualitatively similar to each other. The overall spread ΔT is $\sim$3.5 K which is similar to that for the B-P(a300) sample. The temperature variation of H_{hf} for the C-P sample is also similar to that for the B-P(300) and the C-S samples.

4. Discussion

By combining the results obtained by magnetization, ac-susceptibility and Mössbauer measurements, we try to explain how the transition from the paramagnetic to the antiferromagnetic state is actualized in $FeBr_2$. We focus our attention on the anomalous behaviours observed just below T_p, because T_p not T_N signifies the magnetic transition in $FeBr_2$.

We propose the following model. When the sample is cooled to T_p, Fe^{2+} spins do not form actual AF long-range order (AF-LRO) but rather AF domains. Most of the AF domains fluctuate faster than $\sim 10^{-7}$ s (Larmor precession time of the ^{57}Fe relevant nuclear spin in $FeBr_2$ ($H_{hf} \sim 30$ kOe)), and Fe^{2+} spins belonging to such AF domains give the paramagnetic doublet in the Mössbauer spectrum. On the other hand, there is a small amount of large domains that establish the AF-LRO network at T_p. The spins forming the AF-LRO at T_p give the magnetically split Mössbauer spectrum. When the temperature decreases below T_p, some of the AF domains combine with one another and are put into the AF-LRO. Thus, the number of spins belonging to the AF-LRO increases with decreasing temperature, which results in the increase of the ratio of the Mössbauer magnetic spectrum. This process terminates at T_{EP}, which is supported by the fact that below T_{EP} the Mössbauer spectrum consists of only the magnetic spectrum.

On the other hand, the excess magnetization M_{EX} appearing under the FC condition can be attributed to the AF domains having magnetic moments as a whole originating from unpaired spins between layers. We call such AF domains 'odd domains' for the sake of convenience, regardless of whether the real number of spins consisting of the AF domain is even or odd. If the 'odd domains' fluctuate quickly, they do not contribute to M_{EX}, because the magnetic moment is averaged over the measurement time and is zero. As the temperature decreases below T_p, the AF domains are incorporated into the AF-LRO one by one, in which case, the magnetic moment of the 'odd domain' should be oriented as parallel to H_{dc} as possible to reduce

magnetic energy. Thus, such 'odd-domains' become to contribute to M_{EX}, and M_{EX} increases. However, M_{EX} turns to decrease at T_{EP} suggesting the occurrence of some phenomenon. Here we recall that the imaginary part of ac-susceptibilities χ'' shows a sharp peak at T_{EP} (figure 2). In addition, in the M_{ZFC}–T and χ'–T curves, a small but obvious anomaly is seen also at T_{EP} (figures 1 and 2). These facts suggest the occurrence of some kind of cooperative transition in the spin system. We infer the origin of these phenomena to be as follows. Above T_{EP}, there still remain some disorders within the AF-LRO network, most of which are formed at moments when the AF domains are incorporated within the AF-LRO. When the temperature reaches T_{EP}, rearrangements of the spins occur cooperatively in the AF-LRO network so as to reduce the disorders, and a large amount of exchange mismatches among spins on the boundaries of the AF domains incorporated disappear. As a result, the number of 'odd domains', and accordingly the number of spins contributing to M_{EX}, considerably decreases. It is of particular interest to us that the paramagnetic component in the Mössbauer spectrum disappears around T_{EP}, that is $\Delta T \cong T_p - T_{EP}$. This fact strongly suggests that the anomalous temperature variation of the magnetization, ac-susceptibility and Mössbauer spectrum are commonly attributed to the dynamical behaviour of the AF domains before the spin system establishes the actual LRO.

Here, we point out that a sharp peak is observed in the χ''–T curve at T_p in addition to that at T_{EP}. This is also anomalous and indicates that the transition at T_p of $FeBr_2$ is different from that in ordinary antiferromagnets in which χ'' does not show a peak at T_N. Thus, we identify that the temperature T_p especially defined in the present work has an important meaning to signify the onset of the magnetic ordering in $FeBr_2$. As mentioned above, at T_p the AF domains are formed and most of them are fluctuating faster than the Mössbauer timescale (10^{-7} s). Our observation is consistent with the phenomenon that the critical fluctuations are observed by the neutron scattering experiment over a rather wide temperature region extending to temperatures a little above T_N.

5. Summary

We have demonstrated that $FeBr_2$ transforms from the paramagnetic to antiferromagnetic state through the intermediate AF domain state, which exists at the temperature region between T_p and T_{EP}. As shown above, T_{EP} varies from sample to sample. We consider that the stacking fault of the anion layers is closely related to the formation of the intermediate AF domain state. Thus, we infer that the existence of the stacking fault prevents immediate establishment of the actual LRO at T_N or T_p due to irregularities of the exchange paths created at the locations of the stacking faults. As the temperature decreases, the thermal average of the spins become large and the strength of the exchange coupling overcomes the disturbance due to the stacking fault. Thus, rearrangement of the spins occurs which lowers the exchange energy of the whole spin system by reducing the disorders between the spins on the boundaries of the domains. Although T_{EP} is sample dependent, we are confident that our detection of the intermediate AF domain state is not a trivial matter. We believe that a similar transition process is detected in other magnets in which lattice defects are inherently introduced: magnetic compounds of the CdI_2-type and $CdCl_2$-type are the most prominent candidates.

Acknowledgments

We are grateful to W Kleemann for invaluable discussions. We are also grateful to K Katsumata and H Aruga Katori for helpful discussion and for kindly providing the sample C-S. We thank T Tamaki for her collaboration at the early stage of the Mössbauer measurements. This work

was supported in part by a Grant-in-Aid for Scientific Research from the Japanese Ministry of Education, Science, Sports and Culture.

References

[1] Lanusse M C, Carrara P, Fert A R, Mischler G and Redoulès J P 1972 *J. Physique* **33** 429
[2] Fert A R, Carrara P, Lanusse M C, Mischler G and Redoules J P 1973 *J. Phys. Chem. Solids* **34** 223
[3] Bertrand Y, Fert A R and Gelard J 1974 *J. Physique* **35** 385
[4] Pouget S 1993 *PhD Thesis* INSA, Toulouse
[5] Pelloth J, Brand R A, Takele S, de Azevedo M M P, Kleemann W, Binek Ch, Kushauer J and Bertrand D 1995 *Phys. Rev.* B **52** 15372
[6] Fujita T, Ito A and Ono K 1969 *J. Phys. Soc. Japan* **27** 1143
[7] Ito A and Di N-L 1999 *J. Phys. Soc. Japan* **68** 1098
[8] Aruga Katori H, Katsumata K and Katori M 1996 *Phys. Rev.* B **54** R-9620
[9] Binek Ch, de Azevedo M M P, Kleemann W and Bertrand D 1995 *J. Magn. Magn. Mater.* **140–144** 1555
[10] de Azevedo M M P, Binek Ch, Kushauer J, Kleemann W and Bertrand D 1995 *J. Magn. Magn. Mater.* **140–144** 1557